

# P2T: Pyramid Pooling Transformer for Scene Understanding

Yu-Huan Wu, Yun Liu, Xin Zhan, and Ming-Ming Cheng

**Abstract**—This paper jointly resolves two problems in vision transformer: i) the computation of Multi-Head Self-Attention (MHSA) has high computational/space complexity; ii) recent vision transformer networks are overly tuned for image classification, ignoring the difference between image classification (simple scenarios, more similar to NLP) and downstream scene understanding tasks (complicated scenarios, rich structural and contextual information). To this end, we note that pyramid pooling has been demonstrated to be effective in various vision tasks owing to its powerful ability in context abstraction, and its natural property of spatial invariance is also suitable to address the loss of structural information (problem ii). Hence, we propose to adapt pyramid pooling to MHSA for alleviating its high requirement on computational resources (problem i). In this way, this pooling-based MHSA can well address the above two problems and is thus flexible and powerful for downstream scene understanding tasks. Plugged with our pooling-based MHSA, we build a downstream-task-oriented transformer network, dubbed Pyramid Pooling Transformer (P2T). Extensive experiments demonstrate that, when applied P2T as the backbone network, it shows substantial superiority in various downstream scene understanding tasks such as semantic segmentation, object detection, instance segmentation, and visual saliency detection, compared to previous CNN- and transformer-based networks. The code will be released at <https://github.com/yuhuan-wu/P2T>.

**Index Terms**—Transformer, backbone network, pyramid pooling, scene understanding, downstream tasks

## 1 INTRODUCTION

IN the past decade, convolutional neural networks (CNNs) have dominated computer vision and achieved many great stories [1]–[8]. The state of the arts of various vision tasks on many large-scale datasets has been significantly pushed forward [9]–[13]. In an orthogonal field, *i.e.*, natural language processing (NLP), the dominating technique is transformer [14]. Transformer entirely relies on self-attention to capture the long-range global relationships and has achieved brilliant successes. Considering that global information is also essential for vision tasks, a proper adaption of the transformer [14] should be useful to overcome the limitation of CNNs, *i.e.*, CNNs usually enlarge the receptive field through stacking more layers.

Lots of efforts are dedicated to exploring such a proper adaption of the transformer [14]. Some early attempts use CNNs [2], [4] to extract deep features that are fed into transformers for further processing and regressing the targets [15]–[17]. Dosovitskiy *et al.* [18] made a thorough success by applying a pure transformer network for image classification. They split an image into patches and took each patch as a word/token in an NLP application so that transformer can then be directly adopted. This simple method attains competitive performance on ImageNet [9]. Therefore, a new concept of vision transformer appears. In a very short period, a large amount of literature has emerged to improve

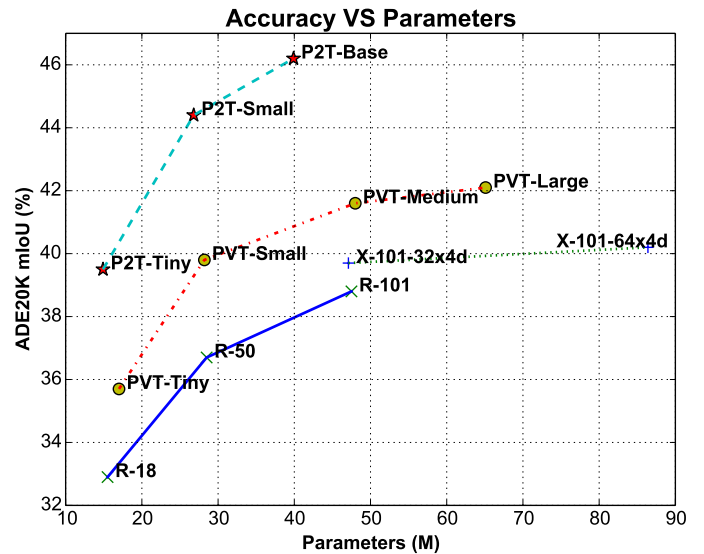


Fig. 1. Experimental comparison for semantic segmentation on the ADE20K dataset [13]. Following PVT [20], Semantic FPN [24] is chosen as the basic method, equipped with different backbone networks, including PVT [20], ResNets [4], ResNeXt [25], and our P2T.

vision transformer [18], and much better performance than CNNs has been achieved [19]–[23]. Nevertheless, there are two obvious problems still existed in vision transformer.

The first problem is about the length of data sequence. When viewing image patches as tokens, the sequence length is much longer than that in NLP applications. Since the computational and space complexity of Multi-Head Self-Attention (MHSA) in the transformer is *quadratic* (rather than *linear* in CNNs) to the image size, directly applying the transformer to vision tasks has a high requirement

- Y.-H. Wu and M.-M. Cheng are with TKLNDST, College of Computer Science, Nankai University, Tianjin, China. (E-mail: wuyuhuan@mail.nankai.edu.cn, cmm@nankai.edu.cn)
- Y. Liu is with Computer Vision Lab, ETH Zurich, Switzerland. (E-mail: yun.liu@vision.ee.ethz.ch)
- X. Zhan is with Alibaba Group. (E-mail: zhanxin.zx@alibaba-inc.com)
- The first two authors contributed equally to this work.
- Corresponding author: M.-M. Cheng. (E-mail: cmm@nankai.edu.cn)
- This work is done while Y.-H. Wu is a research intern of Alibaba Group.

for computational resources. To make a pure transformer network possible for image classification, Dosovitskiy *et al.* [18] used large patch sizes, *e.g.*, 16 and 32, for reducing the sequence length. However, downstream vision tasks usually have higher-resolution inputs than image classification, and such large patches are also suboptimal, especially for dense prediction tasks, because many details would be lost. To address this problem, PVT [20] directly downsamples the feature map in the computation of MHSA. In fact, it models token-to-region relationship rather than the expected token-to-token relationship. Swin Transformer [21] proposes to compute MHSA within small windows rather than across the whole input, modeling local relationships. It uses a window shift strategy to gradually enlarge the receptive field, like CNNs, enlarging the receptive field through stacking more layers. However, the most essential characteristic of vision transformer is its *direct global relationship modeling*, which is also the reason why we transfer from CNNs to transformers.

The other problem is about the domain gap between computer vision and NLP. It is common sense that image 2D structures are essential for vision tasks, while for NLP, only the order of sequence matters. The order of sequence can be simply handled by a position embedding [14] that, however, cannot represent 2D structures. Unfortunately, most of recent development on transformer focuses on improving image classification on ImageNet [1] without considering this problem [19]–[22]. Note that images in the ImageNet dataset [1] only have *simple contexts*, *e.g.*, some objects of the same class centered at the image. A simple position embedding may handle such simple cases well for image-level classification but is obviously suboptimal for complicated real-world scenarios, especially for dense predictions where pixel-level image understanding is required. Therefore, we argue that previous image classification results of vision transformer networks cannot represent their performance in downstream vision tasks. There is an urgent need for a downstream-task-oriented transformer to bridge the domain gap between computer vision and NLP.

This paper aims at resolving the above two problems jointly to promote the usage of the transformer in downstream vision tasks. To this end, we note that pyramid pooling [26], [27] is an effective technique for summarizing long-range information of the deep feature map. Specifically, pyramid pooling adopts multiple pooling operations with different receptive fields and strides onto the input feature map. This simple technique has been demonstrated to be effective in various vision tasks for scene understanding, such as semantic segmentation [27], object detection [26], image super-resolution [28], stereo matching [29], image deraining [30], image dehazing [31], visual saliency detection [32], *etc.* If we can adapt the idea of pyramid pooling to resolving the problem of sequence length in vision transformer, we can perfectly address the abovementioned two problems because pyramid pooling can naturally capture multi-scale/long-range contexts and 2D structures with multi-kernel pooling operations and the spatial invariance of pyramid pooling, respectively.

We achieve this goal by proposing **Pyramid Pooling Transformer (P2T)** for downstream vision tasks. Specifically, we first adapt the idea of pyramid pooling to the

computation of MHSA, which not only reduces the computational load but also captures contextual and structural information. By applying the new pooling-based MHSA, P2T is suitable for downstream vision tasks, unlike previous vision transformers that are mostly tuned for image classification. We evaluate P2T for various typical vision tasks, *i.e.*, semantic segmentation, object detection, instance segmentation, and visual saliency detection. Extensive experiments demonstrate that P2T performs better than all previous CNN- and transformer-based backbone networks in downstream vision tasks (see Fig. 1 for comparisons on semantic segmentation).

In summary, our main contributions include:

- We propose the pooling-based MHSA, which not only significantly reduces the requirement of computational resources but also captures contextual and structural information needed for downstream vision tasks.
- We plug our pooling-based MHSA into the transformer and thus build a downstream-task-oriented transformer network, *i.e.*, P2T, making it flexible and powerful for various downstream scene understanding tasks.
- We conduct extensive experiments to demonstrate that, when applied as a backbone network for various scene understanding tasks, *e.g.*, semantic segmentation, object detection, instance segmentation, and visual saliency detection, P2T achieves substantially better performance than previous CNN- and transformer-based networks.

## 2 RELATED WORK

### 2.1 Convolutional Neural Networks

Since AlexNet [1] won the champion in the ILSVRC-2012 competition [9], numerous advanced techniques have been invented for improving CNNs, achieving many successful stories in computer vision. VGG [2] and GoogleNet [3] first try to deepen CNNs for better image recognition. Then, ResNets [4] succeed in building very deep CNNs with the help of residual connections. ResNeXts [25] and Res2Nets [8] improve ResNets [4] by exploring its cardinal operation. DenseNets [5] introduce dense connections that connect each layer to all its subsequent layers for easing optimization. MobileNets [33], [34] decompose a vanilla convolution into a  $1 \times 1$  convolution and a depthwise separable convolution to build lightweight CNNs for mobile and embedded vision applications. ShuffleNets [35], [36] further reduce the latency of MobileNets [33], [34] by replacing  $1 \times 1$  convolution with grouped  $1 \times 1$  convolution and channel shuffle. EfficientNet [7] and MansNet [37] adopt neural architecture search (NAS) to search for optimal network architectures. Since our work focuses on transformer [14], a comprehensive survey of CNNs is beyond the scope of this paper. Please refer to [38], [39] for a more extensive survey.

### 2.2 Vision Transformer

Transformer is initially proposed for machine translation in NLP [14]. Through MHSA, transformer entirely relies on

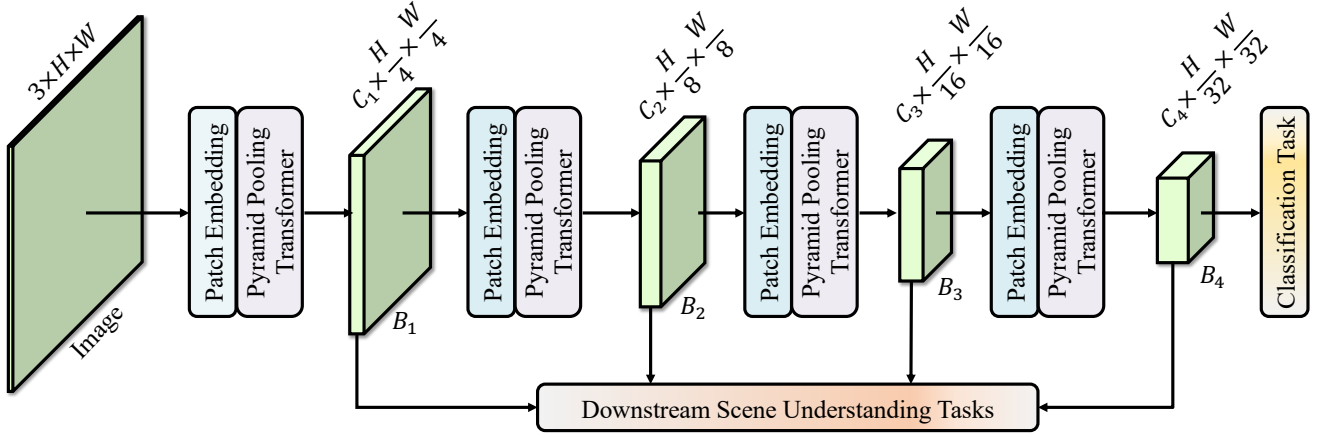


Fig. 2. **Architecture of the proposed P2T network.** We replace the traditional MHSA with our pooling-based MHSA. Features  $\{B_1, B_2, B_3, B_4\}$  can be used for downstream scene understanding tasks.

self-attention to model global token-to-token dependencies. Considering that global relationship is also highly required by computer vision tasks, it is a natural idea to adopt transformer for improving vision tasks. However, transformer is designed to process sequence data and thus cannot process images directly. Hence, some researchers use CNNs to extract 2D representation that is then flattened and fed into transformer [15], [16], [40]–[42]. DETR [15] is a milestone in this direction.

Instead of relying on the CNN backbone for feature extraction, Dosovitskiy *et al.* [18] proposed the first vision transformer (ViT). They split an image into small patches, and each patch is viewed as a word/token in an NLP application. Thus, a pure transformer network can be directly adopted with the class token used for image classification. They achieved competitive performance on ImageNet [9]. Then, DeiT [43] alleviates the required resources for training ViT [18] via knowledge distillation. T2T-ViT [44] proposes to split an image with overlapping to better preserve local structures. Some efforts are contributed to building the pyramid structure for vision transformer using pooling operations [19]–[22]. Among them, PVT [20] adopts a pooling operation to reduce the number of tokens when computing MHSA. Hence, PVT actually does token-to-region relationship modeling, not the expected token-to-token modeling. Since PVT also claims its purpose for downstream tasks, we adopt it as a strong baseline in this paper. Swin Transformer [21] reduces the computational load of MHSA by computing it within small windows. However, Swin Transformer gradually achieves global relationship modeling by window shift, which is somewhat like CNNs that enlarge receptive field by stacking more layers. Hence, we think that Swin Transformer [21] sacrifices the most essential characteristic of vision transformer, *i.e.*, *direct global relationship modeling*.

Different from recent vision transformer networks that are overly tuned for image classification, this paper aims at developing downstream-task-oriented transformer networks. To this end, we have to jointly resolve two problems: i) the high computational/space complexity; ii) domain gap between computer vision and NLP, or that between image classification and downstream scene understanding tasks. Our solution is to adapt the idea of pyramid pooling into

the computation of MHSA. The proposed P2T not only has lower computational/space complexity than typical ViT but also extracts structural and contextual information missed by other transformer competitors. P2T is also compatible with other transformer techniques such as knowledge distillation [43], patch embedding [45], positional encoding [46], and feed-forward network [23], [47].

### 2.3 Pyramid Pooling in CNNs

The concept of pyramid pooling is first proposed by He *et al.* [26] for image classification and object detection. They adopted several pooling operations to pool the final convolutional feature map of a CNN backbone into several fixed-size maps. These resulting maps are then flattened and concatenated into a fixed-length representation for robust visual recognition. Then, Zhao *et al.* [27] applied pyramid pooling for semantic segmentation. Instead of flattening in [26], they upsampled the pooled fixed-size maps into original size and concatenated the upsampled maps for prediction. Their success suggests the effectiveness of pyramid pooling in dense prediction. After that, pyramid pooling has been widely applied to various vision tasks such as semantic segmentation [27], object detection [26], image super-resolution [28], stereo matching [29], image deraining [30], image dehazing [31], visual saliency detection [32], *etc.*

Unlike existing literature that explores pyramid pooling in CNNs for specific tasks, we propose to adapt the concept of pyramid pooling to vision transformer backbone. With this idea, we manage to propose P2T, a flexible and powerful transformer backbone, which can be easily used by various downstream vision tasks. Extensive experiments on semantic segmentation, object detection, instance segmentation, and visual saliency detection demonstrate the superiority of P2T compared with existing CNN- and transformer-based networks.

## 3 METHODOLOGY

In this section, we first provide an overview of our P2T networks in §3.1. Then, we present the architecture of P2T with pooling-based MHSA in §3.2. Finally, we introduce some implementation details of our networks in §3.3.

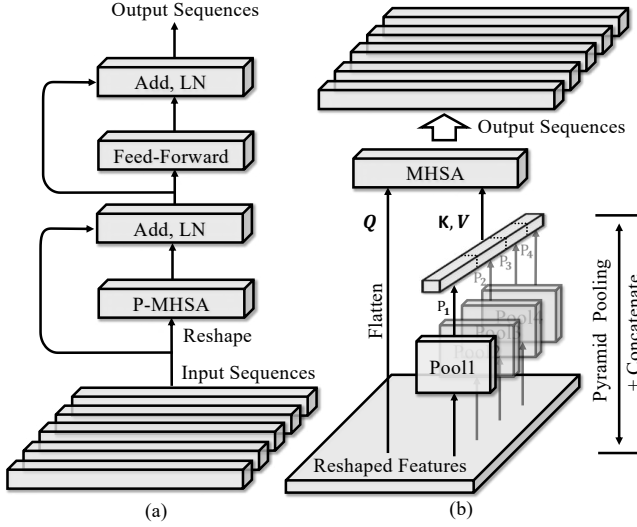


Fig. 3. **Illustration of Pyramid Pooling Transformer.** (a) The brief structure of Pyramid Pooling Transformer. (b) The detailed structure of the pooling-based MHSA.

### 3.1 Overview

The overall architecture of P2T is illustrated in Fig. 2. With a natural color image as input, P2T first splits it into  $\frac{H}{4} \times \frac{W}{4}$  patches, each of which is flattened to 48 ( $4 \times 4 \times 3$ ) elements. Following [20], we feed these flattened patches to a patch embedding module, which consists of a linear projection layer followed by the addition with a learnable positional encoding. The patch embedding module will expand the feature dimension from 48 to  $C_1$ . Then, we stack the proposed pyramid pooling transformer blocks that will be introduced in the next part (§3.2). The whole network can be divided into four stages with feature dimensions of  $C_i$  ( $i = \{1, 2, 3, 4\}$ ), respectively. Between every two stages, each  $2 \times 2$  patch group is concatenated and linearly projected from  $4 \times C_i$  to  $C_{i+1}$  dimension ( $i = \{1, 2, 3\}$ ). In this way, the scales of four stages become  $\frac{H}{4} \times \frac{W}{4}$ ,  $\frac{H}{8} \times \frac{W}{8}$ ,  $\frac{H}{16} \times \frac{W}{16}$ , and  $\frac{H}{32} \times \frac{W}{32}$ , respectively. For four stages, we can derive four feature representations  $\{\mathbf{B}_1, \mathbf{B}_2, \mathbf{B}_3, \mathbf{B}_4\}$ , respectively. For image classification, only  $\mathbf{B}_4$  will be used for final prediction; while for downstream scene understanding tasks, all pyramid features can be utilized.

### 3.2 Pyramid Pooling Transformer

Pyramid pooling has been widely used in many downstream scene understanding tasks collaborating with CNNs [26]–[32], [48]–[50]. However, existing literature usually applies pyramid pooling on top of CNN backbones for extracting global and contextual information for a specific task. In contrast, this paper is the first to explore pyramid pooling in transformers and backbone networks, targeting for improving various downstream scene understanding tasks. To this end, we adapt the idea of pyramid pooling to the transformer for not only reducing the computational load of MHSA but also capturing contextual and structural information.

Let us continue by introducing the proposed P2T, the structure of which is illustrated in Fig. 3 (a). The input first passes through the pooling-based MHSA, whose output is

added with the residual identity, followed by LayerNorm [51]. Like the traditional transformer block [18], [20], [43], a feed-forward network (FFN) follows for feature projection. A residual connection and LayerNorm [51] are applied again. The above process can be formulated as

$$\begin{aligned} \mathbf{X}_{att} &= \text{LayerNorm}(\mathbf{X} + \text{P-MHSA}(\mathbf{X})), \\ \mathbf{X}_{out} &= \text{LayerNorm}(\mathbf{X}_{att} + \text{FFN}(\mathbf{X}_{att})), \end{aligned} \quad (1)$$

where  $\mathbf{X}$ ,  $\mathbf{X}_{att}$ , and  $\mathbf{X}_{out}$  are the input, the output of MHSA, and the output of the transformer block, respectively. P-MHSA is the abbreviation of pooling-based MHSA.

#### 3.2.1 Pooling-based MHSA

Here we present the design of our pooling-based MHSA. Its structure is shown in Fig. 3 (b). First, the input  $\mathbf{X}$  is reshaped into the 2D space. Then, we apply multiple average pooling layers with various ratios onto the reshaped  $\mathbf{X}$  to generate pyramid feature maps, like

$$\begin{aligned} \mathbf{P}_1 &= \text{AvgPool}_1(\mathbf{X}), \\ \mathbf{P}_2 &= \text{AvgPool}_2(\mathbf{X}), \\ &\dots, \\ \mathbf{P}_n &= \text{AvgPool}_n(\mathbf{X}), \end{aligned} \quad (2)$$

where  $\{\mathbf{P}_1, \mathbf{P}_2, \dots, \mathbf{P}_n\}$  denote the generated pyramid feature maps and  $n$  is the number of pooling layers. Then, we feed pyramid feature maps to depthwise convolution for relative positional encoding:

$$\mathbf{P}_i^{enc} = \text{DWConv}(\mathbf{P}_i) + \mathbf{P}_i, \quad i = 1, 2, \dots, n, \quad (3)$$

where  $\text{DWConv}(\cdot)$  indicates the depthwise convolution with kernel size  $3 \times 3$ , and  $\mathbf{P}_i^{enc}$  is  $\mathbf{P}_i$  with relative positional encoding. Since  $\mathbf{P}_i$  are pooled features, such operations in Equ. 3 has little computational cost. Next, we flatten and concatenate these pyramid feature maps:

$$\mathbf{P} = \text{LayerNorm}(\text{Concat}(\mathbf{P}_1^{enc}, \mathbf{P}_2^{enc}, \dots, \mathbf{P}_n^{enc})), \quad (4)$$

where the flattening operation is omitted for simplicity. In this way,  $\mathbf{P}$  can be a shorter sequence than the input  $\mathbf{X}$  if pooling ratios are large enough. Besides,  $\mathbf{P}$  contains global contextual abstraction of the input and can thus serve as a strong substitute for the input when computing MHSA.

Suppose the query, key, and value tensors in MHSA [18] are  $\mathbf{Q}$ ,  $\mathbf{K}$ , and  $\mathbf{V}$ , respectively. Instead of using traditional

$$(\mathbf{Q}, \mathbf{K}, \mathbf{V}) = (\mathbf{X}\mathbf{W}^q, \mathbf{X}\mathbf{W}^k, \mathbf{X}\mathbf{W}^v), \quad (5)$$

we propose to use

$$(\mathbf{Q}, \mathbf{K}, \mathbf{V}) = (\mathbf{X}\mathbf{W}^q, \mathbf{P}\mathbf{W}^k, \mathbf{P}\mathbf{W}^v), \quad (6)$$

in which  $\mathbf{W}^q$ ,  $\mathbf{W}^k$ , and  $\mathbf{W}^v$  denote the weight matrices of linear transformations for generating the query, key, and value tensors, respectively. Then,  $\mathbf{Q}$ ,  $\mathbf{K}$ ,  $\mathbf{V}$  are fed into the attention module to compute the attention  $\mathbf{A}$ , which can be formulated as below:

$$\mathbf{A} = \text{Softmax}\left(\frac{\mathbf{Q} \times \mathbf{K}^T}{\sqrt{d_K}}\right) \times \mathbf{V}, \quad (7)$$

where  $d_K$  is the channel dimension of  $\mathbf{K}$ , and  $\sqrt{d_K}$  can serve as an approximate normalization. The Softmax function is applied along the rows of the matrix. Equ. 7 omits the concept of multiple heads [14], [18] for simplicity.

Since the  $\mathbf{K}$  and  $\mathbf{V}$  have a smaller length than  $\mathbf{X}$ , the proposed P-MHSA is more efficient than traditional MHSA [14], [18]. Besides, since  $\mathbf{K}$  and  $\mathbf{V}$  contains highly-abstracted multi-scale information, the proposed P-MHSA has a stronger capability in global contextual dependency modeling, which is helpful for scene understanding [26]–[32]. From a different perspective, pyramid pooling is usually used as an effective technique connected upon backbone networks; in contrast, this paper first exploits pyramid pooling within backbone networks through transformers, thus providing powerful feature representation learning for scene understanding. With the above analyses, P-MHSA is expected to be more efficient and more effective than traditional P-MHSA [14], [18].

### 3.2.2 Feed-Forward Network

Feed-Forward Network (FFN) is an essential component of transformers for feature enhancement [14], [52]. Previous transformers usually apply an MLP as the FFN [14], [18], [20] and entirely rely on attention to capture inter-pixel dependencies. Though effective, this architecture is not good at learning locality and translation-invariant representations, which play a critical role in scene understanding. To this end, we follow [23] to insert convolution operations into FFN so that the resulting transformer can inherit the merits of both transformer (*i.e.*, long-range dependency modeling) and CNN (*i.e.*, locality and translation-invariance). Specifically, we adopt the Inverted Bottleneck Block (IRB), proposed in MobileNetV2 [34], as the FFN.

To adapt IRB for vision transformer, we first transform the input sequence  $\mathbf{X}_{att}$  to a 2D feature map  $\mathbf{X}_{att}^I$ :

$$\mathbf{X}_{att}^I = \text{Seq2Image}(\mathbf{X}_{att}), \quad (8)$$

where  $\text{Seq2Image}(\cdot)$  is to reshape the 1D sequence to a 2D feature map. Given the input  $\mathbf{X}_{att}^I$ , IRB can be directly applied, like

$$\begin{aligned} \mathbf{X}_{IRB}^1 &= \text{Act}(\mathbf{X}_{att}^I \mathbf{W}_{IRB}^1), \\ \mathbf{X}_{IRB}^{\text{out}} &= \text{Act}(\text{DWConv}(\mathbf{X}_{IRB}^1)) \mathbf{W}_{IRB}^2, \end{aligned} \quad (9)$$

where  $\mathbf{W}_{IRB}^1, \mathbf{W}_{IRB}^2$  indicate the weight matrices of  $1 \times 1$  convolutions, “Act” indicates the nonlinear activation function,  $\mathbf{X}_{IRB}^{\text{out}}$  is the output of IRB. Since  $\mathbf{X}_{IRB}^{\text{out}}$  is a 2D feature map, we finally transform it to a 1D sequence:

$$\mathbf{X}_{IRB}^S = \text{Image2Seq}(\mathbf{X}_{IRB}^{\text{out}}), \quad (10)$$

where  $\text{Image2Seq}(\cdot)$  is the operation that reshapes the 2D feature map to a 1D sequence.  $\mathbf{X}_{IRB}^S$  is the final output of FFN, with the same shape as  $\mathbf{X}_{att}$ .

## 3.3 Implementation Details

**P2T with different depths.** Following previous backbone architectures [4], [20], [21], [23], [25], we build P2T with different depths via stacking different number of pyramid pooling transformers at each stage. In this manner, we propose three versions of P2T, *i.e.*, P2T-Tiny, P2T-Small, and P2T-Base, with similar numbers of parameters to ResNet-18 [4], ResNet-50 [4], and ResNet-101 [4], respectively. The details of depths at each stage for different versions of P2T are shown in Table 1.

TABLE 1  
Detailed settings of the proposed P2T.

Parameters	#Stage			
	1	2	3	4
Number of Attention Heads	1	2	5	8
FFN Expansion Ratio	8	8	4	4
Feature Channels	64	128	320	512
Feature Stride	4	8	16	32
Number of Transformers (P2T-Tiny)	2	2	2	2
Number of Transformers (P2T-Small)	2	2	9	3
Number of Transformers (P2T-Base)	2	4	19	3

TABLE 2  
Experimental results on the validation set of the ADE20K dataset [13] for semantic segmentation by replacing the backbone of Semantic FPN [24]. The number of GFlops is calculated with the input size of  $512 \times 512$ .

Backbone	Semantic FPN [24]		
	#Param (M)	GFlops	mIoU (%)
ResNet-18 [4]	15.5	31.9	32.9
PVT-Tiny [20]	17.0	32.1	35.7 (+2.8)
<b>P2T-Tiny (Ours)</b>	<b>14.9</b>	<b>31.8</b>	<b>39.5 (+6.6)</b>
ResNet-50 [4]	28.5	45.4	36.7
PVT-Small [20]	28.2	42.9	39.8 (+3.1)
<b>P2T-Small (Ours)</b>	<b>26.8</b>	<b>41.7</b>	<b>44.4 (+7.7)</b>
ResNet-101 [4]	47.5	64.8	38.8
ResNeXt-101-32x4d [25]	47.1	64.6	39.7 (+0.9)
PVT-Medium [20]	48.0	59.4	41.6 (+2.8)
<b>P2T-Base (Ours)</b>	<b>39.9</b>	<b>57.5</b>	<b>46.2 (+7.4)</b>

**Pyramid pooling setting.** We empirically set the number of parallel pooling operations in P-MHSA as 4. At different stages, the pooling ratios of the pyramid pooling transformer are different. The pooling ratios for the first stage are empirically set as  $\{12, 16, 20, 24\}$ . Pooling ratios in each next stage are divided by 2 except that in the last stage they are set as  $\{1, 2, 3, 4\}$ . In each transformer block for each stage, we share the parameters of all depthwise convolutions in P-MHSA.

**Other settings.** Although a larger kernel size (*e.g.*,  $5 \times 5$ ) of depthwise convolution can bring better performance, the kernel size of all depthwise convolutions is set to  $3 \times 3$  for efficiency. We choose Hardswish [53] as the nonlinear activation function because it saves much memory compared with GELU [54]. Hardswish [53] also empirically works well. We summarize other P2T settings for each stage in Table 1.

## 4 EXPERIMENTS

Since P2T is specially designed as backbone networks for scene understanding in various downstream vision tasks, we first validate its effectiveness on semantic segmentation, object detection, instance segmentation, and visual saliency detection in §4.1, §4.2, §4.3, and §4.4, respectively. Then, we introduce the experiments on image classification in §4.5. At last, we conduct ablation studies for better understanding our method in §4.6.

### 4.1 Semantic Segmentation

Given an natural image input, semantic segmentation aims at assigning a semantic label to each pixel. It is one of

the most fundamental dense prediction tasks in computer vision.

**Experimental setup.** We evaluate P2T and its competitors on the ADE20K [13] and Cityscapes [12] datasets. The ADE20K dataset is a challenging scene understanding dataset with 150 fine-grained semantic classes. In this dataset, there are 20000, 2000, and 3302 images for training, validation, and testing, respectively. The Cityscapes dataset is another challenging dataset, which consists of 5000 high-quality images of  $1024 \times 2048$  resolution. All images are divided into 2975 training, 500 validation, and 1525 testing images. Following [20], Semantic FPN [24] is chosen as the basic method for a fair comparison. We replace the backbone of Semantic FPN [24] with various network architectures. All backbones of semantic FPN have been pretrained on the ImageNet-1K [9] dataset, and other layers are initialized using the Xavier method [55]. All networks are trained for 80000 iterations. We apply AdamW [56] as the network optimizer, with the initial learning rate of  $1e-4$  and weight decay of 0.01. A *poly* learning rate schedule with  $\gamma = 0.9$  is adopted. Each mini-batch has 16 images for both datasets. Images are resized and randomly cropped to  $512 \times 512$  and  $512 \times 1024$  for ADE20K and Cityscapes datasets during training, respectively. Synchronized batch normalization across GPUs is also enabled. During testing, images are resized to the shorter side of 512 and 1024 for ADE20K and Cityscapes datasets, respectively. Multi-scale testing and flipping are disabled. We use the MMSeg [57] toolbox to implement the above experiments.

**Experimental results on ADE20K.** Table 2 shows the evaluation results on the ADE20K dataset [13]. We compare our proposed P2T with ResNets [4], ResNeXts [25], and PVTs [20]. Benefiting from the pyramid pooling technique, the results of Semantic FPN [24] with our P2T backbone are much better than other competitors. Typically, as shown in Table 2, the smallest version of P2T, P2T-Tiny, achieves a much higher (+6.6%) mIoU than ResNet-18 [4] with less model complexity and computational cost. In contrast, PVT-Tiny [20] only has a 2.8% improvement than ResNet-18 [4] with more parameters and computational cost. Increasing the model complexity, P2T-Small has a significant 7.7% improvement compared to ResNet-50 [4] with fewer parameters (26.8M *vs.* 28.5M) and less computational cost (41.7G *vs.* 45.4G). In contrast, the transformer competitor, PVT-Small [20], only has a 3.1% improvement over ResNet-18 [4]. If we continue increasing the complexity of various backbones, P2T-Base still works well and has a 7.4% improvement compared to ResNet-101 [4] with the advantages of less model complexity and computational cost. In contrast, the CNN competitor, ResNeXt-101-32x4d [25], only has a 0.9% improvement, and the transformer competitor, PVT-Medium [20], only has a 2.8% improvement.

**Experimental results on Cityscapes.** For the Cityscapes dataset [12], the proposed P2T still outperforms other competitors by a large margin, as shown in Table 3. Specifically, P2T-Tiny achieves a 5.6% higher mIoU than PVT-Tiny [20]. Surprisingly, PVT-Tiny is even 1.5% and 0.7% better than ResNet-101 [4] and PVT-Medium [20], respec-

TABLE 3

Experimental results on the validation set of the Cityscapes dataset [12]. It is surprising that our tiny backbone, *i.e.*, P2T-Tiny, is even better than ResNet-101 [4] and PVT-Medium [20].

Backbone	Semantic FPN [24]	
	#Param (M)	mIoU (%)
PVT-Tiny [20]	17.0	71.7
<b>P2T-Tiny (Ours)</b>	<b>14.9</b>	<b>77.3 (+5.6)</b>
ResNet-50 [4]	28.5	74.5
PVT-Small [20]	28.2	75.5 (+1.0)
<b>P2T-Small (Ours)</b>	<b>26.8</b>	<b>78.6 (+4.1)</b>
ResNet-101 [4]	47.5	75.8
PVT-Medium [20]	48.0	76.6 (+0.8)
<b>P2T-Base (Ours)</b>	<b>39.9</b>	<b>79.7 (+3.9)</b>

TABLE 4

Object detection results with RetinaNet [58] on the MS-COCO val2017 set [10]. "R" and "X" represent the ResNet [4] and ResNeXt [25], respectively.

Backbone	#Param (M)	RetinaNet [58]					
		AP <sup>b</sup>	AP <sup>b</sup> <sub>50</sub>	AP <sup>b</sup> <sub>75</sub>	AP <sub>S</sub>	AP <sub>M</sub>	AP <sub>L</sub>
R-18 [4]	21.3	31.8	49.6	33.6	16.3	34.3	43.2
PVT-Tiny [20]	23.0	36.7	56.9	38.9	22.6	38.8	50.0
<b>P2T-Tiny (Ours)</b>	<b>20.9</b>	<b>39.3</b>	<b>59.8</b>	<b>41.6</b>	<b>23.0</b>	<b>43.0</b>	<b>52.6</b>
R-50 [4]	37.7	36.3	55.3	38.6	19.3	40.0	48.8
PVT-Small [20]	34.2	40.4	61.3	43.0	25.0	42.9	55.7
<b>P2T-Small (Ours)</b>	<b>32.8</b>	<b>43.2</b>	<b>64.0</b>	<b>46.3</b>	<b>26.6</b>	<b>47.4</b>	<b>58.6</b>
R-101 [4]	56.7	38.5	57.8	41.2	21.4	42.6	51.1
X-101-32x4d [25]	56.4	39.9	59.6	42.7	22.3	44.2	52.5
PVT-Medium [20]	53.9	41.9	63.1	44.3	25.0	44.9	57.6
<b>P2T-Base (Ours)</b>	<b>45.9</b>	<b>44.7</b>	<b>65.8</b>	<b>47.4</b>	<b>27.2</b>	<b>48.6</b>	<b>60.9</b>
X-101-64x4d [25]	95.5	41.0	60.9	44.0	23.9	45.2	54.0
PVT-Large [20]	71.1	42.6	63.7	45.4	25.8	46.0	58.4

tively. The above results suggest that P2T is much more efficient and powerful than ResNets [4] and PVTs [20] for semantic segmentation. PVT-Small and PVT-Medium [20] are only 1.0% and 0.8% better than ResNet-50 and ResNet-101 [4], respectively, while P2T-Small and P2T-Base achieve 4.1% and 3.9% performance gains, respectively. Overall, P2T achieves substantially superior results compared to ResNets [4], ResNeXts [25], and PVTs [20] on the Cityscapes dataset.

**Visual results.** We visually compare P2T-Small to PVT-Small [20] on the Cityscapes dataset [12]. Visualizations are shown in Fig. 4. We can observe that Semantic FPN [24] with the P2T-Small backbone obtains results with higher semantic consistency.

## 4.2 Object Detection

Object detection is also one of the most fundamental and challenging tasks for decades in computer vision. It aims to detect and recognize instances of semantic objects of certain classes in natural images. Here, we evaluate P2T and its competitors on the MS-COCO [10] and PASCAL VOC [11] datasets.

**Experimental setup on MS-COCO.** MS-COCO [10] dataset is a large-scale challenging dataset for object detection, instance segmentation, and keypoint detection. MS-COCO *train*2017 (118k images) and *val*2017 (5k images)

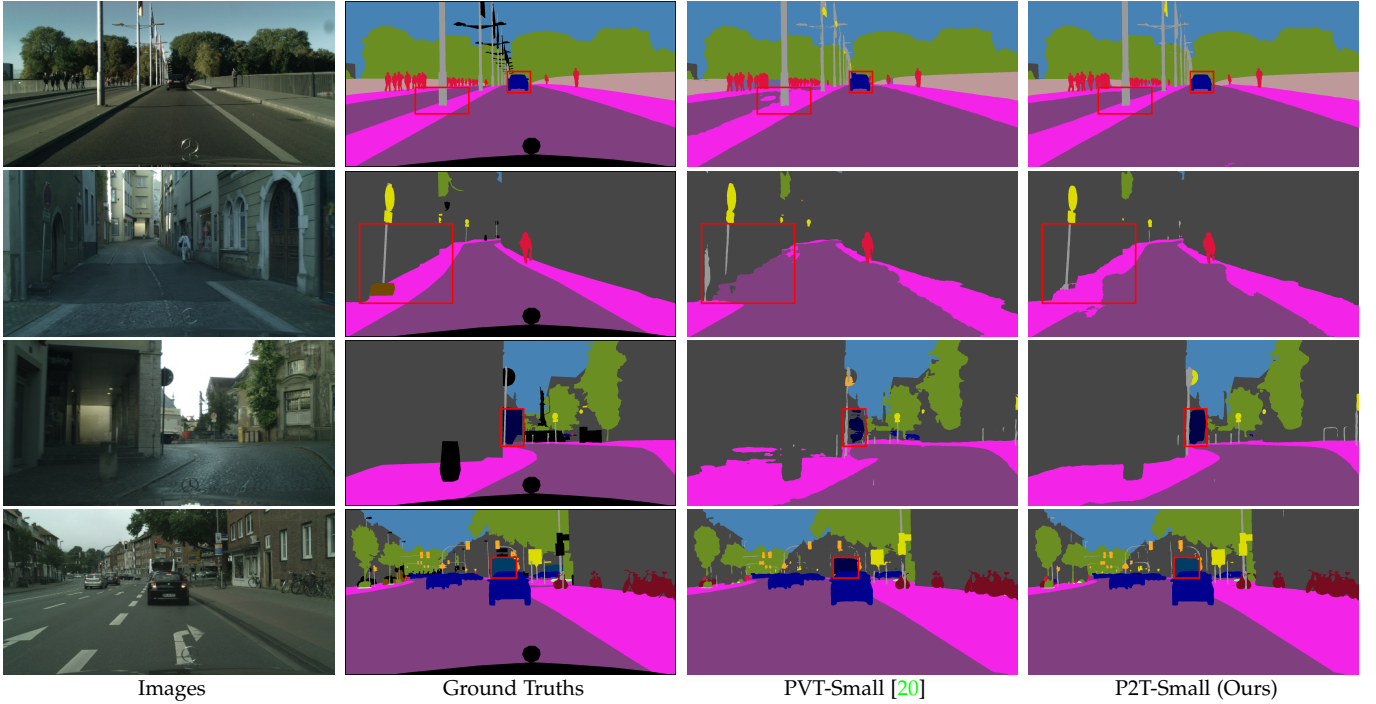


Fig. 4. Visual comparisons on the Cityscapes dataset [12]. The base method is Semantic FPN [24]. Results show that P2T-Small can effectively enhance the semantic consistency compared with PVT-Small [20]. Best viewed in color.

sets are used for training and validation in our experiments, respectively. RetinaNet [58] is applied as the basic framework because it has been widely acknowledged by this community. Each mini-batch has 16 images with an initial learning rate of  $1e-4$ . Following the popular MMDetection toolbox [59], we train each network for 12 epochs, and the learning rate is divided by 10 after 8 and 11 epochs. The network optimizer is AdamW [56], which is a popular optimizer for training transformers. During training and testing, the shorter side of input images is resized to 800 pixels. The longer side will keep the ratio of the images and within 1333 pixels. Only random horizontal flipping is used for data augmentation. Standard COCO API is utilized for evaluation, and we report results in terms of  $AP^b$ ,  $AP_{50}^b$ ,  $AP_{75}^b$ ,  $AP_S$ ,  $AP_M$ , and  $AP_L$  metrics, where “b” indicates the bounding box.  $AP_S$ ,  $AP_M$ , and  $AP_L$  mean AP scores for small, medium, and large objects, respectively.  $AP^b$  is usually viewed as the primary metric.

**Experimental setup on PASCAL VOC.** PASCAL VOC dataset [11] is a popular, typical, and high-quality dataset for object detection. In our experiments, we use this dataset to further validate the generality and effectiveness of the proposed P2T in object detection. We train the well-known Faster R-CNN [60] framework with different backbones on VOC 2007+2012 *trainval* set (16551 images). We evaluate the performance on the VOC 2007 *test* set (4952 images). The training settings are very similar to that of MS-COCO dataset, except that 1) the input size of the shorter side is changed to 600 pixels, and the longer side will keep ratio of the images and within 800 pixels; 2) the learning rate is divided by 10 after 9 epochs; 3) for data augmentation, horizontal flipping is replaced with random cropping. Moreover, the standard evaluation metric for PASCAL VOC

TABLE 5  
Detection results on the PASCAL VOC 2007 test set [11].

Backbone	Faster R-CNN + FPN [61]	
	#Param (M)	mAP (%)
ResNet-18 [4]	28.4	75.7
PVT-Tiny [20]	29.9	79.1 (+3.4)
<b>P2T-Tiny (Ours)</b>	<b>27.9</b>	<b>83.0 (+7.3)</b>
ResNet-50 [4]	41.5	80.1
ResNet-101 [4]	60.6	81.6 (+1.5)
PVT-Small [20]	41.2	82.1 (+2.0)
ResNeXt-101-32x4d [25]	60.3	82.2 (+2.1)
<b>P2T-Small (Ours)</b>	<b>39.9</b>	<b>84.8 (+4.7)</b>

TABLE 6  
Instance segmentation results with Mask R-CNN [62] on the MS-COCO *val*<sub>2017</sub> set [10]. “R” and “X” represent the ResNet [4] and ResNeXt [25], respectively.

Backbone	#Param (M)	Mask R-CNN [62]					
		$AP^b$	$AP_{50}^b$	$AP_{75}^b$	$AP^m$	$AP_{50}^m$	$AP_{75}^m$
R-18 [4]	31.2	34.0	54.0	36.7	31.2	51.0	32.7
PVT-Tiny [20]	32.9	36.7	59.2	39.3	35.1	56.7	37.3
<b>P2T-Tiny (Ours)</b>	<b>30.8</b>	<b>41.2</b>	<b>64.1</b>	<b>44.6</b>	<b>38.1</b>	<b>61.1</b>	<b>40.6</b>
R-50 [4]	44.2	38.0	58.6	41.4	34.4	55.1	36.7
PVT-Small [20]	44.1	40.4	62.9	43.8	37.8	60.1	40.3
<b>P2T-Small (Ours)</b>	<b>42.7</b>	<b>45.2</b>	<b>67.8</b>	<b>49.3</b>	<b>40.9</b>	<b>64.3</b>	<b>44.0</b>
R-101 [4]	63.2	40.4	61.1	44.2	36.4	57.7	38.8
X-101-32x4d [25]	62.8	41.9	62.5	45.9	37.5	59.4	40.2
PVT-Medium [20]	63.9	42.0	64.4	45.6	39.0	61.6	42.1
<b>P2T-Base (Ours)</b>	<b>55.8</b>	<b>46.5</b>	<b>68.2</b>	<b>51.0</b>	<b>41.7</b>	<b>65.1</b>	<b>44.9</b>
X-101-64x4d [25]	101.9	42.8	63.8	47.3	38.4	60.6	41.3
PVT-Large [20]	81.0	42.9	65.0	46.6	39.5	61.9	42.5

is mAP under the IoU threshold of 0.5.

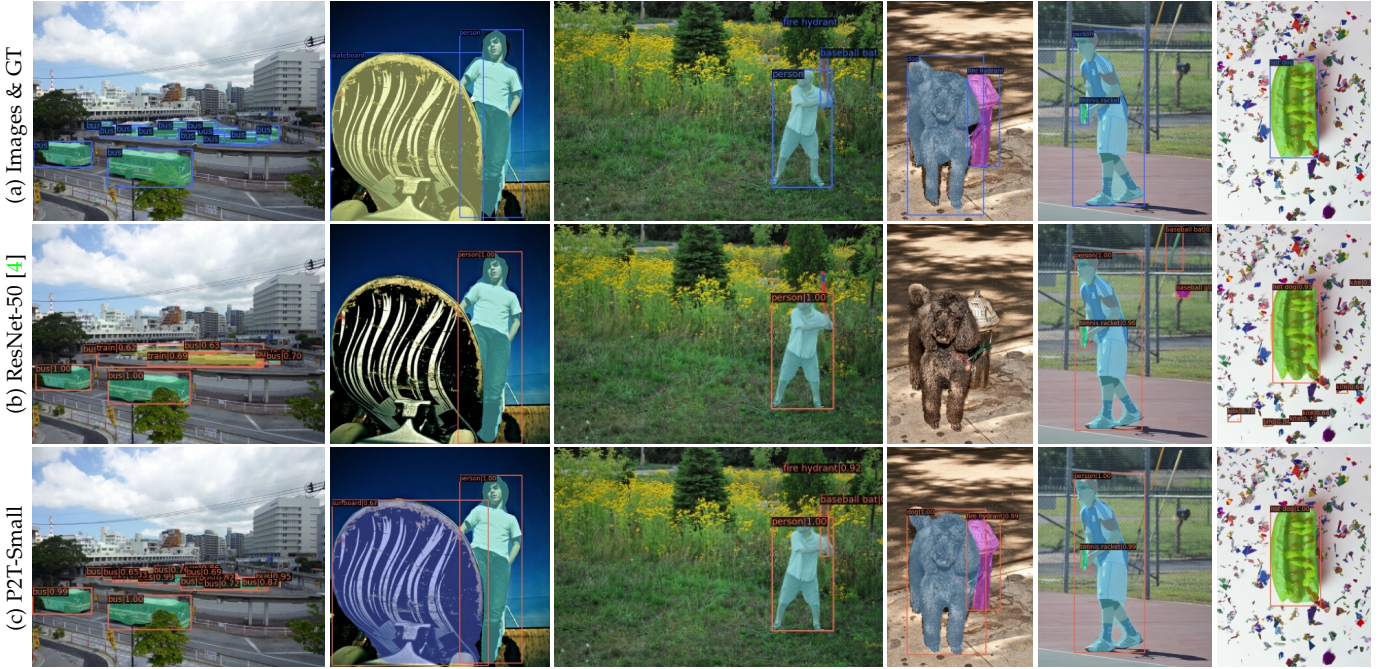


Fig. 5. Visual examples generated by Mask R-CNN [62] with ResNet-50 [4] and the proposed P2T-Small backbones. Benefited from our strong backbone, Mask R-CNN can precisely detect and segment various sizes of objects in clutter, while ResNet-50 [4] cannot. Best viewed in color.

**Experimental results on MS-COCO.** Evaluation results on the MS-COCO dataset are summarized in Table 4. We can observe that our P2T always achieves much better performance with different complexity levels. For example, the tiny version, P2T-Tiny, has a 7.5% and a 2.6% improvement compared with ResNet-18 [4] and PVT-Tiny [20], respectively. P2T-Small is 6.9% and 2.8% better than ResNet-50 [4] and PVT-Small [20], respectively. The largest version of P2T, *i.e.*, P2T-Base, also has a very significant improvement, *i.e.*, +6.2%, +4.8%, and +2.8% than ResNet-101 [4], ResNeXt-101-32x4d [25], and PVT-Medium [20], respectively. Overall, on the MS-COCO dataset, the proposed P2T largely outperforms its CNN competitors, *i.e.*, ResNets [4] and ResNeXts [25], and the transformer competitor PVTs [20].

**Experimental results on PASCAL VOC.** Evaluation results on the PASCAL VOC dataset [11] are presented in Table 5. P2T-Tiny achieves 83.0% mAP, while ResNet-18 [4] and PVT-Tiny [20] are 7.3% and 3.9% lower. It is more surprising that P2T-Tiny is even 2.9%, 1.4%, 0.9%, and 0.8% better than ResNet-50 [4], ResNet-101 [4], PVT-Small [20], and ResNeXt-101-32x4d [25], respectively. Note that P2T-Tiny is just our smallest model designed for mobile platforms. Moreover, PVT-Small [20] has a 2.0% improvement than ResNet-50 [4], while P2T-Small has a much larger 4.7% improvement. The above analyses demonstrate the superiority of the proposed P2T in representation learning when compared to previous CNN and transformer competitors.

### 4.3 Instance Segmentation

Instance segmentation is another advanced challenging task. It can be regarded as a special case of object detection by outputting object masks instead of bounding boxes in object detection.

**Experimental setup.** We evaluate the performance of instance segmentation on the well-known MS-COCO dataset [10]. MS-COCO train2017 and val2017 sets are used for training and validation in our experiments. Mask R-CNN [62] is applied as the basic framework by using different backbone networks. The training settings are the same as what we use for object detection in §4.2. We report evaluation results for both object detection and instance segmentation in terms of  $AP^b$ ,  $AP_{50}^b$ ,  $AP_{75}^b$ ,  $AP^m$ ,  $AP_{50}^m$ , and  $AP_{75}^m$  metrics, where “b” and “m” indicate bounding box and mask metrics, respectively.  $AP^b$  and  $AP^m$  are set as the primary evaluation metrics.

**Experimental results.** The comparisons between P2T and its competitors are displayed in Table 6. Similar to the conclusion of object detection, P2T achieves the best performance consistently compared to existing CNN and transformer backbone networks. Specifically, in terms of bounding box metrics, P2T-Tiny/Small/Base are 7.2%, 7.2%, and 6.1% better than ResNet-18/50/101 [20], respectively. P2T also largely outperforms PVT [20] by 4.5%, 4.8%, and 4.5% on the corresponding Tiny/Small/Base versions with fewer parameters, respectively. In terms of mask metrics, our largest P2T-Base achieves 41.7% mask AP, while the mask AP of the best competitor, PVT-Medium [20], is 2.7% lower. The mask AP of the tiny version of P2T, P2T-Tiny, is 3.0% better than that of the corresponding model, PVT-Tiny [20]. The consistent and significant improvement in the above experiments demonstrates that the feature representations learned by the proposed P2T are more powerful than existing backbone networks in instance segmentation.

**Visual examples.** We present visual examples of Mask R-CNN with ResNet-50 [4] and P2T-Small backbones in Fig. 5. For better visualization, only instances whose confidence

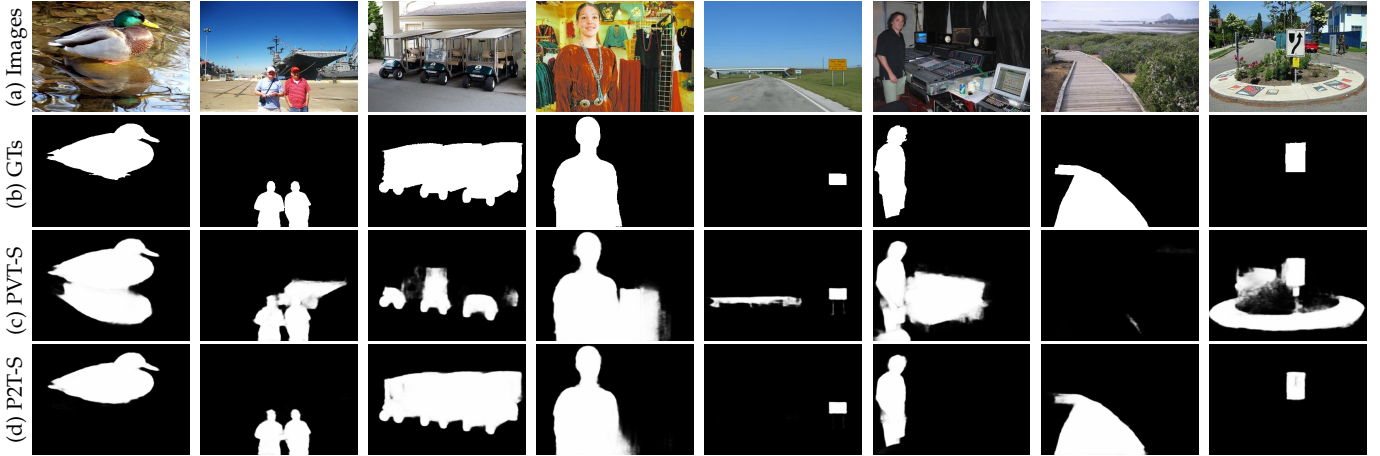


Fig. 6. Qualitative comparison of visual saliency detection. PVT-S [20] and P2T-S indicate PVT-Small and P2T-Small, respectively. Our predictions are more similar to the ground-truth (GT), while PVT-Small [20] would detect wrong or miss salient objects.

TABLE 7  
Evaluation results on DUTS-TE [63], DUT-OMRON (DUT-O) [64], and PASCAL-S [65] datasets for visual saliency detection.

Backbone	#Param (M)	DUTS-TE		DUT-O		PASCAL-S	
		$F_{\max}$	MAE	$F_{\max}$	MAE	$F_{\max}$	MAE
R-18 [4]	14.0	.853	.044	.769	.056	.854	.071
PVT-Tiny [20]	16.0	.876	.039	.813	.052	.868	.067
<b>P2T-Tiny (Ours)</b>	<b>13.4</b>	<b>.895</b>	<b>.033</b>	<b>.825</b>	<b>.048</b>	<b>.883</b>	<b>.059</b>
R-50 [4]	26.9	.873	.038	.786	.051	.864	.065
R-101 [4]	45.9	.879	.036	.797	.049	.876	.060
X-101-32x8d [25]	92.3	.889	.033	.808	.047	.871	.059
PVT-Small [20]	27.3	.900	.032	.832	.050	.883	.060
<b>P2T-Small (Ours)</b>	<b>25.1</b>	<b>.912</b>	<b>.029</b>	<b>.840</b>	<b>.045</b>	<b>.898</b>	<b>.053</b>

score is larger than 0.6 are presented. We can observe that, with P2T as the backbone, Mask R-CNN [62] works well on various scenes with object occlusions and small objects in clutter, while Mask R-CNN [62] with ResNet-50 [4] may detect and segment wrong instances, or miss obvious objects.

#### 4.4 Visual Saliency Detection

Visual saliency detection is a fundamental task in computer vision, which tries to simulate the human visual system to detect the most salient and eye-attracting region/objects in natural images.

**Experimental setup.** Since U-Net [66] like decoders are with simple structures and without complicated aggregation paths, we use the U-Net [66] decoder with the SCPC block [67] as the basic framework for visual saliency detection. Following recent popular works [49], [67]–[70], the 10553 images in the DUTS training (DUTS-TR) set [63] are for training. Three most popular and challenging datasets, *i.e.*, DUTS testing (DUTS-TE) set (5019 images) [63], DUT-OMRON [64] (5168 images), and PASCAL-S [65] (850 images), are for evaluation. During training, we only apply random resizing-cropping and horizontal flipping as data augmentation. Each mini-batch has 24 images. The input image is resized to  $384 \times 384$  during training and testing. We train each network for 30 epochs. The Adam [71] optimizer is used for all backbones, with the learning rate of 5e-

5,  $\beta_1$  of 0.9, and  $\beta_2$  of 0.99. Deep supervision is enabled during training. A combination of binary cross entropy loss and Dice loss [72] is applied. Two most popular and basic metrics, *i.e.*, maximum F-measure and mean absolute error (MAE), are applied as evaluation metrics. Please refer to [67] for more details about the above two metrics.

**Experimental results.** We summarize the evaluation results in Table 7. Comparing to PVT [20], we can observe that, with P2T as the backbone, models can much more precisely detect salient objects in terms of both F-measure and MAE scores, as P2T-Tiny/Small largely outperforms PVT-Tiny/Small with fewer parameters. A surprising result is that P2T-Tiny beats ResNet-50/101 [4] and even ResNeXt-101-32x4d [25], demonstrating that P2T is much more effective than ResNet [4] and ResNeXt [25] for visual saliency detection.

**Visual results.** We visually compare P2T to the transformer backbone PVT-Small [20], as shown in Fig. 6. While P2T-Small can completely segment salient objects in various scenes with object occlusions or low contrast, PVT-Small [20] is easy to miss parts of objects, detect wrong salient regions, and even report no salient regions. Such behavior shows that our P2T can catch global relationships and precisely perform saliency reasoning more effectively.

#### 4.5 Image Classification

Image classification is the most common task for evaluating the capability of backbone networks. It aims to assign a class label to each input natural image. Many other tasks build on top of image classification via applying networks for image classification as the backbones of them. Since our motivation is to design a downstream-task-oriented network, improving the accuracy of image classification is not our main focus.

**Experimental setup.** As described in §3.1, only the output feature  $\mathbf{B}_4$  of the last stage is utilized here. Following regular CNN networks [4], [5], [8], we append a global average pooling layer and a fully-connected layer on top of  $\mathbf{B}_4$  to obtain the final classification scores. We train our network

TABLE 8

Image classification results on the ImageNet-1K dataset [9]. “R” and “X” represent ResNet [4] and ResNeXt [25], respectively. “Top-1” indicates the top-1 error rate (the lower, the better). “\*” indicates the results with knowledge distillation. The number of GFlops is reported with the input size of  $224 \times 224$ .

Method	#Param (M)	GFlops	Top-1 (%)
R-18 [4]	11.7	1.8	31.5
DeiT-Tiny/16* [43]	5.7	1.3	27.8
PVT-Tiny [20]	13.2	1.9	24.9
<b>P2T-Tiny (Ours)</b>	<b>11.1</b>	<b>1.9</b>	<b>21.9</b>
R-50 [4]	25.6	4.1	21.5
X-50-32x4d [25]	25.0	4.3	20.5
DeiT-Small/16* [43]	22.1	4.6	20.1
PVT-Small [20]	24.5	3.8	20.2
<b>P2T-Small (Ours)</b>	<b>23.0</b>	<b>3.6</b>	<b>17.9</b>
R-101 [4]	44.7	7.9	20.2
X-101-32x4d [25]	44.2	8.0	19.4
X-101-64x4d [25]	83.5	15.6	18.5
ViT-Small/16 [18]	48.8	9.9	19.2
ViT-Base/16 [18]	86.6	17.6	18.2
DeiT-Base/16* [43]	86.6	17.6	18.2
PVT-Medium [20]	44.2	6.7	18.8
PVT-Large [20]	61.4	9.8	18.3
<b>P2T-Base (Ours)</b>	<b>36.2</b>	<b>6.3</b>	<b>17.0</b>

on the ImageNet-1K dataset [9], which has 1.28M training images and 50k validation images. For a fair comparison, we follow [20] to adopt the same training protocols as DeiT [43], which is a standard choice for training transformers. Specifically, we use AdamW [56] as the optimizer, with the learning rate of  $1e-4$  and a mini-batch of 1024 images. We train P2T for 300 epochs with the cosine learning rate decay strategy. Images are resized to a size of  $224 \times 224$  for training and testing. Models are warmed up for the five beginning epochs. The data augmentation is also the same as [20], [43].

**Experimental results.** The quantitative comparisons are summarized in Table 8. Although we do not focus on image classification, P2T achieves superior results compared with recent state-of-the-art transformer models. For example, P2T-Small has a significant 2.3% improvement over PVT-Small [20] with fewer parameters (23.0M *vs.* 24.5M) and less computational cost (3.6G *vs.* 3.8G). P2T-Base is 1.8% better than PVT-Medium [20] with fewer parameters (36.2M *vs.* 44.2M). P2T also largely outperforms ViT [18] and DeiT [43] with much fewer parameters, implying that P2T achieves better performance without a large amount of training data and knowledge distillation. Therefore, P2T is also very capable for image classification.

#### 4.6 Ablation Studies

**Experimental setup.** In this section, we perform ablation studies to analyze the efficacy of each design choice. We evaluate the performance of model variants on semantic segmentation and image classification. Due to the limited computational resources, we only train each model variant on the ImageNet dataset [9] for 100 epochs, while other training settings keep the same as in §4.5. Then, we fine tune the ImageNet-pretrained model on the ADE20K dataset [13] with the same training settings in §4.1.

TABLE 9

Ablation study on pyramid pooling and IRB. “Top-1” indicates the top-1 error rate on the ImageNet-1K dataset [9] for image classification (the lower, the better). “mIoU” is the mean IoU rate on the ADE20K dataset [13] for semantic segmentation (the higher, the better).

Baseline	P-MHSA	IRB	Top-1 (%)	mIoU (%)
✓			26.2	35.0
✓	✓		23.5	38.3
✓	✓	✓	20.5	42.7

TABLE 10

Ablation study on the pooling ratios and fixed pooled size. GFlops is computed with an input size of  $512 \times 512$  for the semantic segmentation model, *i.e.*, Semantic FPN [24]. Memory (Mem) denotes the training GPU memory usage for Semantic FPN [24] with a batch size of 2. “†” indicates to use fixed pooled size rather than fixed pooling ratios.

Pooling Ratios	GFlops	Mem (GB)	Top-1 (%)	mIoU (%)
{12, 16, 20, 24}	41.7	3.9	20.5	42.7
{16, 20, 24, 32}	40.7	3.7	20.6	42.1
{1, 2, 3, 6}†	39.0	3.5	20.7	41.7

**Pyramid pooling and IRB.** To validate the effectiveness of P-MHSA and IRB, we set a baseline that i) replaces P2T’s P-MHSA with an MHSA with a single pooling operation and ii) replaces IRB with a regular MLP as in most transformers [20], [43]. Experimental results are shown in Table 9. After applying pyramid pooling, the performance is largely improved. An extra depthwise convolution in the feed-forward network, *i.e.*, IRB, also shows significant improvement, demonstrating the necessity of the locality enhancement in the feed-forward network.

**Pooling ratios.** We also try larger pooling ratios for saving more computational cost. The results are shown in Table 10. We find that using larger pooling ratios, *i.e.*, {16, 20, 24, 32}, will result in a 0.6% performance drop on semantic segmentation and a 0.1% top-1 accuracy drop on image classification. Therefore, P2T is not very sensitive to the setting of pooling ratios.

**Fixed pooled size.** When using fixed pooling ratios, the size of the pooled feature map will vary with the input feature map. Here, we try to fix the pooled size as {1, 2, 3, 6} for all stages, using adaptive average pooling. The results are shown in Table 10. Compared with our default setting, about 10% memory usage and 6.5% computational cost are saved. However, the top-1 classification accuracy drops 0.2%, and the semantic segmentation performance is 1.0% lower. Hence, we choose to use fixed pooling ratios rather than fixed pooled size.

**GELU *vs.* Hardswish.** We use the Hardswish function [53] for nonlinear activation to reduce GPU memory usage in the training phase. Typically, when we train P2T on ImageNet with a batch size of 32, the GPU memory usage of GELU [54] is 4.8GB, which is 1GB (26%) more than that of Hardswish [53]. We also find that there is no obvious accuracy change if we employ Hardswish [53].

## 5 CONCLUSION

To alleviate the high computational cost of MHSA in vision transformer, this paper proposes pooling-based MHSA by adapting the pyramid pooling technique into MHSA. Since pyramid pooling has the natural properties of spatial invariance and contextual abstraction, our pooling-based MHSA is not only flexible but also powerful for downstream scene understanding tasks. Equipped with the pooling-based MHSA, we construct a downstream-task-oriented backbone network, called Pyramid Pooling Transformer (P2T). To demonstrate its effectiveness, we conduct extensive experiments on several typical downstream tasks, including semantic segmentation, object detection, instance segmentation, and visual saliency detection. Experimental results suggest that P2T largely outperforms previous CNN- and transformer-based networks. P2T also achieves competitive performance for image classification on the ImageNet dataset [9].

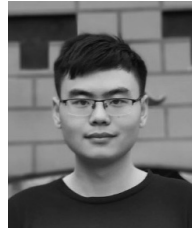
## ACKNOWLEDGEMENT

This work is supported by the Alibaba research intern program.

## REFERENCES

- [1] A. Krizhevsky, I. Sutskever, and G. E. Hinton, "Imagenet classification with deep convolutional neural networks," in *Adv. Neural Inform. Process. Syst.*, 2012, pp. 1097–1105.
- [2] K. Simonyan and A. Zisserman, "Very deep convolutional networks for large-scale image recognition," in *Int. Conf. Learn. Represent.*, 2015.
- [3] C. Szegedy, W. Liu, Y. Jia, P. Sermanet, S. Reed, D. Anguelov, D. Erhan, V. Vanhoucke, and A. Rabinovich, "Going deeper with convolutions," in *IEEE Conf. Comput. Vis. Pattern Recog.*, 2015, pp. 1–9.
- [4] K. He, X. Zhang, S. Ren, and J. Sun, "Deep residual learning for image recognition," in *IEEE Conf. Comput. Vis. Pattern Recog.*, 2016, pp. 770–778.
- [5] G. Huang, Z. Liu, G. Pleiss, L. Van Der Maaten, and K. Weinberger, "Convolutional networks with dense connectivity," *IEEE Trans. Pattern Anal. Mach. Intell.*, 2019.
- [6] J. Hu, L. Shen, S. Albanie, G. Sun, and E. Wu, "Squeeze-and-excitation networks," *IEEE Trans. Pattern Anal. Mach. Intell.*, vol. 42, no. 8, pp. 2011–2023, 2020.
- [7] M. Tan and Q. Le, "EfficientNet: Rethinking model scaling for convolutional neural networks," in *Int. Conf. Mach. Learn.*, 2019, pp. 6105–6114.
- [8] S. Gao, M.-M. Cheng, K. Zhao, X.-Y. Zhang, M.-H. Yang, and P. H. Torr, "Res2Net: A new multi-scale backbone architecture," *IEEE Trans. Pattern Anal. Mach. Intell.*, vol. 43, no. 2, pp. 652–662, 2021.
- [9] O. Russakovsky, J. Deng, H. Su, J. Krause, S. Satheesh, S. Ma, Z. Huang, A. Karpathy, A. Khosla, M. Bernstein *et al.*, "ImageNet large scale visual recognition challenge," *Int. J. Comput. Vis.*, vol. 115, no. 3, pp. 211–252, 2015.
- [10] T.-Y. Lin, M. Maire, S. Belongie, J. Hays, P. Perona, D. Ramanan, P. Dollár, and C. L. Zitnick, "Microsoft COCO: Common objects in context," in *Eur. Conf. Comput. Vis.*, 2014, pp. 740–755.
- [11] M. Everingham, L. Van Gool, C. K. Williams, J. Winn, and A. Zisserman, "The pascal visual object classes (voc) challenge," *Int. J. Comput. Vis.*, vol. 88, no. 2, pp. 303–338, 2010.
- [12] M. Cordts, M. Omran, S. Ramos, T. Rehfeld, M. Enzweiler, R. Benenson, U. Franke, S. Roth, and B. Schiele, "The cityscapes dataset for semantic urban scene understanding," in *IEEE Conf. Comput. Vis. Pattern Recog.*, 2016, pp. 3213–3223.
- [13] B. Zhou, H. Zhao, X. Puig, S. Fidler, A. Barriuso, and A. Torralba, "Scene parsing through ADE20K dataset," in *IEEE Conf. Comput. Vis. Pattern Recog.*, 2017, pp. 633–641.
- [14] A. Vaswani, N. Shazeer, N. Parmar, J. Uszkoreit, L. Jones, A. N. Gomez, Ł. Kaiser, and I. Polosukhin, "Attention is all you need," in *Adv. Neural Inform. Process. Syst.*, 2017, pp. 6000–6010.
- [15] N. Carion, F. Massa, G. Synnaeve, N. Usunier, A. Kirillov, and S. Zagoruyko, "End-to-end object detection with transformers," in *Eur. Conf. Comput. Vis.*, 2020, pp. 213–229.
- [16] X. Zhu, W. Su, L. Lu, B. Li, X. Wang, and J. Dai, "Deformable DETR: Deformable transformers for end-to-end object detection," *arXiv preprint arXiv:2010.04159*, 2020.
- [17] R. Hu and A. Singh, "Transformer is all you need: Multimodal multitask learning with a unified transformer," *arXiv preprint arXiv:2102.10772*, 2021.
- [18] A. Dosovitskiy, L. Beyer, A. Kolesnikov, D. Weissenborn, X. Zhai, T. Unterthiner, M. Dehghani, M. Minderer, G. Heigold, S. Gelly *et al.*, "An image is worth 16x16 words: Transformers for image recognition at scale," *arXiv preprint arXiv:2010.11929*, 2020.
- [19] B. Heo, S. Yun, D. Han, S. Chun, J. Choe, and S. J. Oh, "Rethinking spatial dimensions of vision transformers," *arXiv preprint arXiv:2103.16302*, 2021.
- [20] W. Wang, E. Xie, X. Li, D.-P. Fan, K. Song, D. Liang, T. Lu, P. Luo, and L. Shao, "Pyramid Vision Transformer: A versatile backbone for dense prediction without convolutions," *arXiv preprint arXiv:2102.12122*, 2021.
- [21] Z. Liu, Y. Lin, Y. Cao, H. Hu, Y. Wei, Z. Zhang, S. Lin, and B. Guo, "Swin Transformer: Hierarchical vision transformer using shifted windows," *arXiv preprint arXiv:2103.14030*, 2021.
- [22] H. Fan, B. Xiong, K. Mangalam, Y. Li, Z. Yan, J. Malik, and C. Feichtenhofer, "Multiscale vision transformers," *arXiv preprint arXiv:2104.11227*, 2021.
- [23] Y. Liu, G. Sun, Y. Qiu, L. Zhang, A. Chhatkuli, and L. Van Gool, "Transformer in convolutional neural networks," *arXiv preprint arXiv:2106.03180*, 2021.
- [24] A. Kirillov, R. Girshick, K. He, and P. Dollár, "Panoptic feature pyramid networks," in *IEEE Conf. Comput. Vis. Pattern Recog.*, 2019, pp. 6399–6408.
- [25] S. Xie, R. Girshick, P. Dollár, Z. Tu, and K. He, "Aggregated residual transformations for deep neural networks," in *IEEE Conf. Comput. Vis. Pattern Recog.*, 2017, pp. 1492–1500.
- [26] K. He, X. Zhang, S. Ren, and J. Sun, "Spatial pyramid pooling in deep convolutional networks for visual recognition," *IEEE Trans. Pattern Anal. Mach. Intell.*, vol. 37, no. 9, pp. 1904–1916, 2015.
- [27] H. Zhao, J. Shi, X. Qi, X. Wang, and J. Jia, "Pyramid scene parsing network," in *IEEE Conf. Comput. Vis. Pattern Recog.*, 2017, pp. 2881–2890.
- [28] D. Park, K. Kim, and S. Young Chun, "Efficient module based single image super resolution for multiple problems," in *IEEE Conf. Comput. Vis. Pattern Recog. Worksh.*, 2018, pp. 882–890.
- [29] J.-R. Chang and Y.-S. Chen, "Pyramid stereo matching network," in *IEEE Conf. Comput. Vis. Pattern Recog.*, 2018, pp. 5410–5418.
- [30] H. Zhang, V. Sindagi, and V. M. Patel, "Image de-raining using a conditional generative adversarial network," *IEEE Trans. Circ. Syst. Video Technol.*, vol. 30, no. 11, pp. 3943–3956, 2019.
- [31] H. Zhang and V. M. Patel, "Densely connected pyramid dehazing network," in *IEEE Conf. Comput. Vis. Pattern Recog.*, 2018, pp. 3194–3203.
- [32] T. Wang, A. Borji, L. Zhang, P. Zhang, and H. Lu, "A stagewise refinement model for detecting salient objects in images," in *Int. Conf. Comput. Vis.*, 2017, pp. 4019–4028.
- [33] A. G. Howard, M. Zhu, B. Chen, D. Kalenichenko, W. Wang, T. Weyand, M. Andreetto, and H. Adam, "MobileNets: Efficient convolutional neural networks for mobile vision applications," *arXiv preprint arXiv:1704.04861*, 2017.
- [34] M. Sandler, A. Howard, M. Zhu, A. Zhmoginov, and L.-C. Chen, "MobileNetV2: Inverted residuals and linear bottlenecks," in *IEEE Conf. Comput. Vis. Pattern Recog.*, 2018, pp. 4510–4520.
- [35] N. Ma, X. Zhang, H.-T. Zheng, and J. Sun, "ShuffleNet v2: Practical guidelines for efficient CNN architecture design," in *Eur. Conf. Comput. Vis.*, 2018, pp. 116–131.
- [36] X. Zhang, X. Zhou, M. Lin, and J. Sun, "ShuffleNet: An extremely efficient convolutional neural network for mobile devices," in *IEEE Conf. Comput. Vis. Pattern Recog.*, 2018, pp. 6848–6856.
- [37] M. Tan, B. Chen, R. Pang, V. Vasudevan, M. Sandler, A. Howard, and Q. V. Le, "MnasNet: Platform-aware neural architecture search for mobile," in *IEEE Conf. Comput. Vis. Pattern Recog.*, 2019, pp. 2820–2828.
- [38] A. Khan, A. Sohail, U. Zahoor, and A. S. Qureshi, "A survey of the recent architectures of deep convolutional neural networks," *Artif. Intell. Review*, vol. 53, no. 8, pp. 5455–5516, 2020.

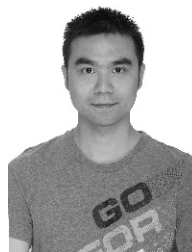
- [39] W. Liu, Z. Wang, X. Liu, N. Zeng, Y. Liu, and F. E. Alsaadi, "A survey of deep neural network architectures and their applications," *Neurocomputing*, vol. 234, pp. 11–26, 2017.
- [40] H. Wang, Y. Zhu, H. Adam, A. Yuille, and L.-C. Chen, "MaX-DeepLab: End-to-end panoptic segmentation with mask transformers," *arXiv preprint arXiv:2012.00759*, 2020.
- [41] R. Liu, Z. Yuan, T. Liu, and Z. Xiong, "End-to-end lane shape prediction with transformers," in *IEEE Winter Conf. Appl. Comput. Vis.*, 2021, pp. 3694–3702.
- [42] J. Hu, L. Cao, L. Yao, S. Zhang, Y. Wang, K. Li, F. Huang, R. Ji, and L. Shao, "ISTR: End-to-end instance segmentation with transformers," *arXiv preprint arXiv:2105.00637*, 2021.
- [43] H. Touvron, M. Cord, M. Douze, F. Massa, A. Sablayrolles, and H. Jégou, "Training data-efficient image transformers & distillation through attention," *arXiv preprint arXiv:2012.12877*, 2020.
- [44] L. Yuan, Y. Chen, T. Wang, W. Yu, Y. Shi, F. E. Tay, J. Feng, and S. Yan, "Tokens-to-Token ViT: Training vision transformers from scratch on ImageNet," *arXiv preprint arXiv:2101.11986*, 2021.
- [45] Z. Jiang, Q. Hou, L. Yuan, D. Zhou, X. Jin, A. Wang, and J. Feng, "Token labeling: Training a 85.5% top-1 accuracy vision transformer with 56M parameters on ImageNet," *arXiv preprint arXiv:2104.10858*, 2021.
- [46] X. Chu, B. Zhang, Z. Tian, X. Wei, and H. Xia, "Do we really need explicit position encodings for vision transformers?" *arXiv preprint arXiv:2102.10882*, 2021.
- [47] Y. Li, K. Zhang, J. Cao, R. Timofte, and L. Van Gool, "LocalViT: Bringing locality to vision transformers," *arXiv preprint arXiv:2104.05707*, 2021.
- [48] P. Zhang, D. Wang, H. Lu, H. Wang, and X. Ruan, "Amulet: Aggregating multi-level convolutional features for salient object detection," in *Int. Conf. Comput. Vis.*, 2017, pp. 202–211.
- [49] J.-J. Liu, Q. Hou, M.-M. Cheng, J. Feng, and J. Jiang, "A simple pooling-based design for real-time salient object detection," in *IEEE Conf. Comput. Vis. Pattern Recog.*, 2019, pp. 3917–3926.
- [50] Y.-H. Wu, Y. Liu, L. Zhang, W. Gao, and M.-M. Cheng, "Regularized densely-connected pyramid network for salient instance segmentation," *IEEE Trans. Image Process.*, vol. 30, pp. 3897–3907, 2021.
- [51] J. L. Ba, J. R. Kiros, and G. E. Hinton, "Layer normalization," *arXiv preprint arXiv:1607.06450*, 2016.
- [52] Y. Dong, J.-B. Cordonnier, and A. Loukas, "Attention is not all you need: Pure attention loses rank doubly exponentially with depth," *arXiv preprint arXiv:2103.03404*, 2021.
- [53] A. Howard, M. Sandler, G. Chu, L.-C. Chen, B. Chen, M. Tan, W. Wang, Y. Zhu, R. Pang, V. Vasudevan *et al.*, "Searching for MobileNetV3," in *Int. Conf. Comput. Vis.*, 2019, pp. 1314–1324.
- [54] D. Hendrycks and K. Gimpel, "Gaussian error linear units (GELUs)," *arXiv preprint arXiv:1606.08415*, 2016.
- [55] X. Glorot and Y. Bengio, "Understanding the difficulty of training deep feedforward neural networks," in *Int. Conf. Artif. Intell. Stat.*, 2010, pp. 249–256.
- [56] I. Loshchilov and F. Hutter, "Decoupled weight decay regularization," in *Int. Conf. Learn. Represent.*, 2017.
- [57] M. Contributors, "MMSegmentation: Openmmlab semantic segmentation toolbox and benchmark," <https://github.com/open-mmlab/mms Segmentation>, 2020.
- [58] T.-Y. Lin, P. Goyal, R. Girshick, K. He, and P. Dollár, "Focal loss for dense object detection," in *Int. Conf. Comput. Vis.*, 2017, pp. 2980–2988.
- [59] K. Chen, J. Wang, J. Pang, Y. Cao, Y. Xiong, X. Li, S. Sun, W. Feng, Z. Liu, J. Xu *et al.*, "MMDetection: Open MMLab detection toolbox and benchmark," *arXiv preprint arXiv:1906.07155*, 2019.
- [60] S. Ren, K. He, R. Girshick, and J. Sun, "Faster R-CNN: Towards real-time object detection with region proposal networks," *IEEE Trans. Pattern Anal. Mach. Intell.*, vol. 39, no. 6, pp. 1137–1149, 2017.
- [61] T.-Y. Lin, P. Dollár, R. Girshick, K. He, B. Hariharan, and S. Belongie, "Feature pyramid networks for object detection," in *IEEE Conf. Comput. Vis. Pattern Recog.*, 2017, pp. 2117–2125.
- [62] K. He, G. Gkioxari, P. Dollár, and R. Girshick, "Mask r-cnn," *IEEE Trans. Pattern Anal. Mach. Intell.*, vol. 42, no. 2, pp. 386–397, 2020.
- [63] L. Wang, H. Lu, Y. Wang, M. Feng, D. Wang, B. Yin, and X. Ruan, "Learning to detect salient objects with image-level supervision," in *IEEE Conf. Comput. Vis. Pattern Recog.*, 2017, pp. 136–145.
- [64] C. Yang, L. Zhang, H. Lu, X. Ruan, and M.-H. Yang, "Saliency detection via graph-based manifold ranking," in *IEEE Conf. Comput. Vis. Pattern Recog.*, 2013, pp. 3166–3173.
- [65] Y. Li, X. Hou, C. Koch, J. M. Rehg, and A. L. Yuille, "The secrets of salient object segmentation," in *IEEE Conf. Comput. Vis. Pattern Recog.*, 2014, pp. 280–287.
- [66] O. Ronneberger, P. Fischer, and T. Brox, "U-Net: Convolutional networks for biomedical image segmentation," in *Med. Image. Comput. Assist. Interv. Springer*, 2015, pp. 234–241.
- [67] Y.-H. Wu, Y. Liu, L. Zhang, and M.-M. Cheng, "EDN: Salient object detection via extremely-downsampled network," *arXiv preprint arXiv:2012.13093*, 2020.
- [68] Y. Liu, M.-M. Cheng, X.-Y. Zhang, G.-Y. Nie, and M. Wang, "DNA: Deeply supervised nonlinear aggregation for salient object detection," *IEEE Trans. Cybernetics*, 2021.
- [69] Y. Liu, Y.-C. Gu, X.-Y. Zhang, W. Wang, and M.-M. Cheng, "Lightweight salient object detection via hierarchical visual perception learning," *IEEE Trans. Cybernetics*, 2020.
- [70] Y. Liu, X.-Y. Zhang, J.-W. Bian, L. Zhang, and M.-M. Cheng, "SAM-Net: Stereoscopically attentive multi-scale network for lightweight salient object detection," *IEEE Trans. Image Process.*, vol. 30, pp. 3804–3814, 2021.
- [71] D. P. Kingma and J. Ba, "Adam: A method for stochastic optimization," in *Int. Conf. Learn. Represent.*, 2015.
- [72] F. Milletari, N. Navab, and S.-A. Ahmadi, "V-Net: Fully convolutional neural networks for volumetric medical image segmentation," in *Int. Conf. 3D Vis.*, 2016, pp. 565–571.



**Yu-Huan Wu** is currently a Ph.D. candidate with College of Computer Science at Nankai University, supervised by Prof. Ming-Ming Cheng. He received his bachelor's degree from Xidian University in 2018. His research interests include computer vision and machine learning.



**Yun Liu** received his bachelor's and doctoral degrees from Nankai University in 2016 and 2020, respectively. Currently, he works as a postdoctoral scholar with Prof. Luc Van Gool at ETH Zurich. His research interests include computer vision and machine learning.



**Xin Zhan** received his bachelor's and doctoral degrees from USTC in 2010 and 2015, respectively. Currently, he works as a researcher of Alibaba AI labs. His research interests include 3D point clouds for autonomous driving.



**Ming-Ming Cheng** received his PhD degree from Tsinghua University in 2012. Then he did two years research fellow with Prof. Philip Torr in Oxford. He is now a professor at Nankai University, leading the Media Computing Lab. His research interests include computer graphics, computer vision, and image processing. He received research awards, including ACM China Rising Star Award, IBM Global SUR Award, and CCF-Intel Young Faculty Researcher Program. He is on the editorial boards of IEEE TIP.